Ligand Recognition in Viral RNA Necessitates Rare Conformational Transitions

Lev Levintov and Harish Vashisth*

Department of Chemical Engineering, University of New Hampshire, Durham 03824, NH, USA

E-mail: harish.vashisth@unh.edu

Abstract

Ribonucleic acids (RNAs) are conformationally flexible molecules that fold into three-dimensional structures and play an important role in different cellular processes as well as in development of many diseases. RNA has therefore become an important target for developing novel therapeutic approaches. The biophysical processes underlying RNA function are often associated with rare structural transitions that play a key role in ligand recognition. In this work, we probe these rarely occurring transitions using non-equilibrium simulations by characterizing the dissociation of a ligand molecule from an HIV-1 viral RNA element. Specifically, we observed base flipping rare events that are coupled with ligand binding/unbinding and also provided mechanistic details underlying these transitions.

Graphical TOC Entry

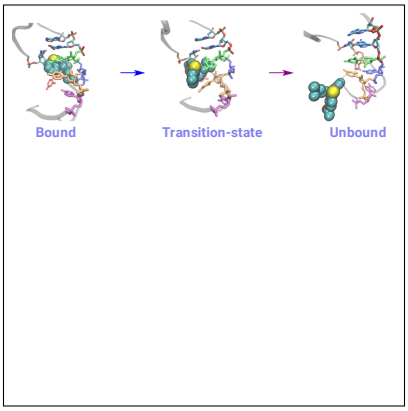

Keywords

Ribonucleic Acid, Viral RNA, Steered Molecular Dynamics, Non-equilibrium Simulations, Jarzynski's Equality

RNA molecules were considered only as passive carriers of genetic information until RNA was implicated in diverse cellular processes (translation and transcription,[1] regulation of gene expression,[2,3] and protein synthesis[4]). Many RNAs are also involved in progression of various diseases including neurological disorders, cancers, and cardiovascular diseases.[5–7] Moreover, RNAs play a critical role in the replication and survival mechanisms of many viruses and bacteria.[8–10] Thus, it is promising to target RNA molecules for developing therapeutic modalities because RNA lies upstream of proteins and its activity can be modulated before or during its synthesis.[11]

Particularly, viral genomes do not provide a large number of protein targets due to the lack of well-defined binding pockets for small molecules.[12] However, conserved and structured RNA motifs of viral genomes are flexible and fold into complex three-dimensional structures that may provide transient binding pockets for small molecules, and thereby activities of "undruggable" proteins could be modulated before they are synthesized.[11,12] For example, new amiloride derivatives were shown to interact with several human immunodeficiency virus type-1 (HIV-1) RNAs and inhibit the replication process of the virus.[13,14]

However, it is more challenging to target RNAs than proteins due to the highly charged nature of the RNA backbone, conformational flexibility of RNA, and a relatively low abundance of cellular RNAs in comparison with the ribosomal RNA.[15] In addition, designing new ligands to target RNA is limited by a poor understanding of the recognition mechanisms between RNA and its binding partners. These mechanisms are important for the function of RNA and the knowledge of the conformational dynamics of binding, as well as their thermodynamic and kinetic properties, will be useful in the drug discovery process.[16]

Experimental techniques including X-ray crystallography and Nuclear Magnetic Resonance (NMR) spectroscopy provide crucial insights into the dynamics of RNA and its interactions with ligands.[17,18] Atomic force microscopy (AFM) is another technique to study interactions between ligands and receptors or unfolding processes by obtaining force-extension data.[19] However, characterization of all possible atomic details of large and complex biomolec-

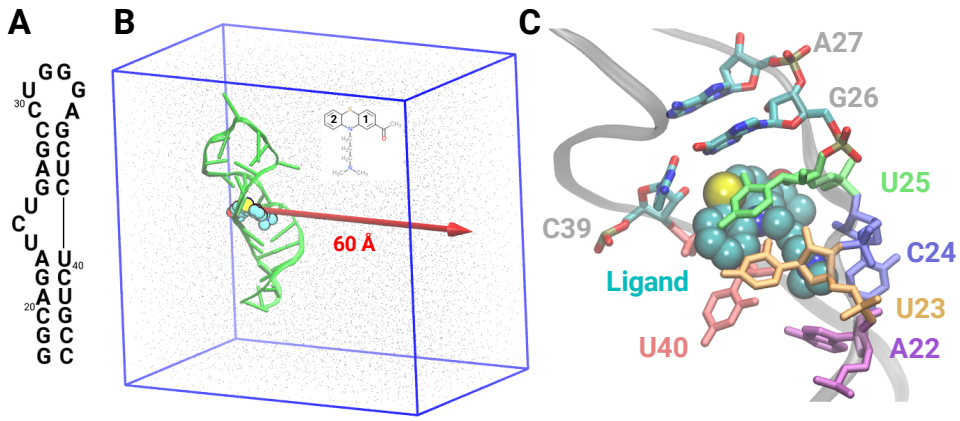

Figure 1: System setup and structural details. (A) Secondary structure of HIV-1 TAR RNA. (B) A side-view of the simulation domain: RNA, green cartoon; water molecules, gray points; ligand, space-filling; and the bounding box, blue. A red arrow indicates the direction of pulling. The chemical structure of the ligand is also shown with labeled aromatic rings (inset). (C) A side view of the binding pocket: ligand is shown in a space-filling representation and each key nucleotide is highlighted in a unique color and labeled.

ular systems continues to be a challenging process for experimental techniques. The number of parameters that need to be measured exceeds the number of parameters that can be tracked in experiments, even with the advanced NMR methods.[20–22]

However, computational methods, such as molecular dynamics (MD) simulations, are becoming increasingly important in characterizing the dynamics of biomolecules and their interactions with ligands by providing additional insights at the atomic level. Although many biophysical processes occur on time-scales challenging to probe using conventional MD simulations, non-equilibrium techniques, such as steered molecular dynamics (SMD) simulations, that enhance conformational sampling are useful in probing critical ligand recognition events. During these processes, interactions that are important for the overall stability of the system are perturbed to reveal key structural motifs involved in ligand binding/unbinding. SMD has been successfully applied to study unfolding of RNA/DNA,[23,24] unbinding mechanisms of protein/ligand,[25,26] RNA/ligand[27,28] complexes, and to study other systems.[29,30]

In this work, we applied MD and SMD simulation methods to study the transactivation response element (TAR) RNA from the HIV-1 (Figure 1A) that is located at the 5′ end of the viral RNA genome. It is a key model system to study RNA dynamics and has been shown to

transition between multiple conformations (e.g. bent and coaxially stacked configurations) along with other less populated states.[22,31] It also has an important function in the viral replication mechanism because it interacts with the viral transactivator (Tat) protein and the host cofactor cyclin T1 to promote efficient transcription of the downstream genome.[32] Therefore, it has been targeted with molecules of various types and sizes and has become a primary drug target in the HIV-1 genome.

Specifically, we conducted a long time-scale MD simulation spanning 2 μs and 300 non-equilibrium SMD simulations (see supporting information) to study the dissociation pathway of a small molecule, acetylpromazine (*inset* in Figure 1B),[33] which represents a compound with low toxicity and high binding affinity with interactions (Figure 1C) in the common binding pocket in TAR-RNA. We now describe results from MD and SMD simulations of acetylpromazine binding/unbinding from TAR-RNA.

Thermodynamics of Ligand Dissociation: The studies of ligand dissociation from bound conformations are most suitably done using non-equilibrium simulations because the system is trapped in an energy minimum with high energy barriers to dissociation where the ligand is stabilized by interactions in the binding pocket. Conventional MD simulations are often non-ergodic due to incomplete sampling and as a result systems usually remain trapped in energy minima. In our work, we did not observe a spontaneous dissociation of acetylpromazine in a conventional and long time-scale (2 μs) MD simulation. As seen in snapshots from the MD trajectory (Figure S1), the ligand remained stably bound to RNA. The buried surface area (BSA), which represents the interface area of contact between the RNA and the ligand, supports this observation since the average BSA is 552 ± 82 Å^2 (Figure S2) with an initial value of 645 Å^2. Thus, observing spontaneous dissociation is a non-trivial task even in μs-long MD simulations and non-equilibrium enhanced sampling methods (e.g. SMD) are needed. We used constant velocity SMD (cv-SMD) simulations for studying the dissociation process of acetylpromazine and for computing the non-equilibrium work of ligand dissociation. The non-equilibrium work values were then used to compute the

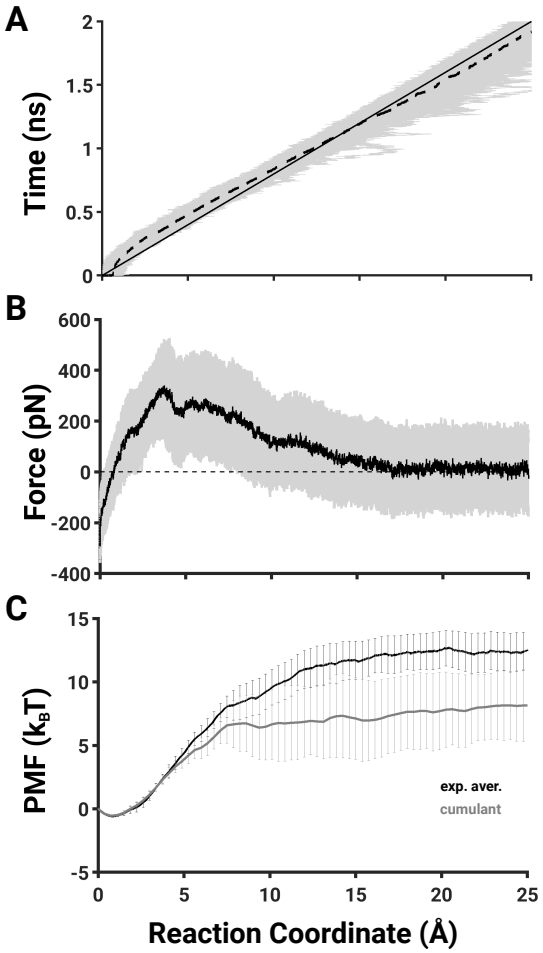

Figure 2: Reaction coordinate, unbinding force, and free-energy from SMD simulations. (A) The COM trajectory of the ligand. Black solid line represents the actual RC, black dotted line represents the average trace across 102 trajectories, and gray lines represent all SMD trajectories. (B) Unbinding force with the mean force (black solid line) and standard deviation profiles (gray) from all SMD simulations are shown. (C) Potential of Mean Force *vs.* RC, as computed using the exponential averaging (black line) and using the second-order cumulant expansion (gray line) with error bars.

unbinding free energy (ΔF) using the exponential averaging as well as the second-order cumulant expansion of the Jarzynski's equality.[34–37] An SMD simulation with the lowest work value will have the highest contribution to the free energy computed via Jarzynski's equality and therefore provides the most valuable information about key interactions that have to be broken or created during the dissociation process since the system requires the least amount of work to overcome those interactions. In contrast, simulations with higher work values provide a less than optimal pathway for ligand dissociation. Thus, the comparison between

simulations requiring the lowest and highest work values can reveal the salient features of the binding/unbinding process of ligands. Specifically, we performed 300 cv-SMD simulations, each 5 ns long, where a harmonic spring with a spring constant $k = 7$ kcal mol^{-1} Å^{-2} was attached to the COM of acetylpromazine and pulled with a velocity of 0.0125 Å/ps along the z-direction. The external work, W (Figure S3), of ligand dissociation from the RNA pocket was computed from 102 trajectories out of all SMD simulations that consistently followed the reaction coordinate (Figure 2A and S4A).

The unbinding cv-SMD force profile (Figure 2B) starts with the ligand in the bound state with no external force applied. Negative forces at the beginning indicate the dominance of system forces over the external force. As the external force values started to increase, overcoming the system forces restricting the ligand to its original conformation, acetylpromazine dissociation begins. The continued increase in the mean force until reaching a maximum value represents the displacements of various nucleotides in the binding pocket and perturbations in stacking interactions between the benzene rings of acetylpromazine and nucleotides. The maximum force corresponds to the point where ligand displaced all nucleotides leading to an open dissociation pathway. A small decrease in the force profile (between 4.3 Å and 4.9 Å) corresponds to a state where both of the benzene rings moved out of the binding pocket. The unbinding forces then decreased as the ligand moved away from the binding pocket. The fluctuations in force were measured after 17.5 Å to ascertain that the average force converged to zero indicating full dissociation of the ligand with no interactions to RNA (Figure S4B).

The free-energy profiles computed using the exponential averaging and second-order cumulant expansion of Jarzynski's equality (Figure 2C) show an energy minimum corresponding to the bound state and converged free-energy values for the unbound state. The free energy difference between the bound and unbound states at 17.5 Å was calculated to be 12.5 ± 1.47 kcal/mol and 8.176 ± 2.87 kcal/mol using the exponential averaging and the second-order cumulant expansion of Jarzynski's equality, respectively. The unbinding free energies were then used to compute the dissociation constant ($K_d = e^{-\frac{\Delta F}{RT}}$, where R is the gas

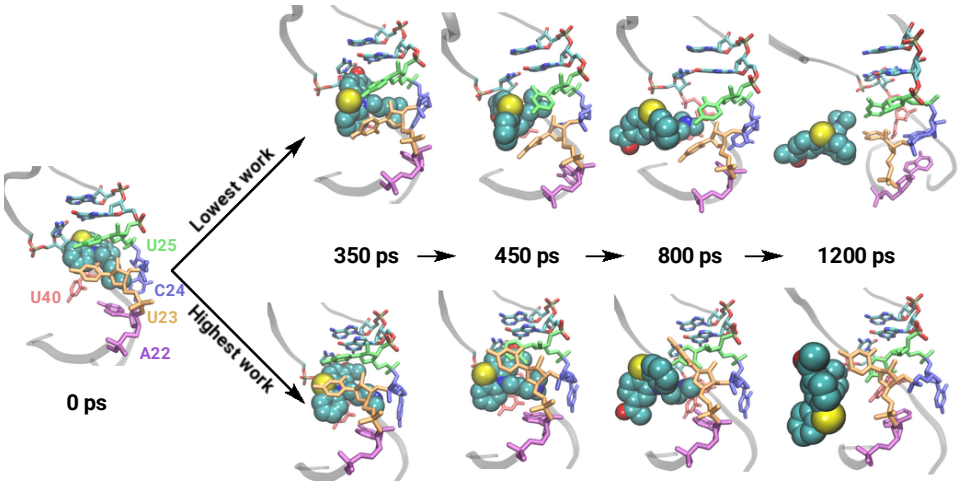

Figure 3: Ligand dissociation mechanism: Snapshots of ligand dissociation from the simulations with the lowest work (top) and the highest work (bottom) are shown. Color and labeling scheme is same as in Figure 1C. See also Figure S6.

constant and T is the temperature) and compared against the experimentally determined values. We estimated K_d value as 1.54 nM (exponential averaging) and 1750 nM (cumulant expansion). The experimental K_d value of 100 nM (corresponding to ∼9.94 kcal/mol) lies within the range of bounds predicted by our simulations.

Ligand Escape Pathway: Initially, the ligand was located between the base pairs G26-C39 and A22-U40 where its benzene ring **2** was inserted between U23, U25 and U40, forming stacking interactions with these bases, and the benzene ring **1** was positioned next to G26, forming an angle of ∼135° to the benzene ring **2**. The aliphatic chain of the ligand was extended along the minor groove of RNA and pushed C24 out of the stack (Figure 1C). We first focused on the dissociation pathway that was observed in the simulation that required to perform the least amount of work out of all SMD trajectories since that simulation has the most important details of the dissociation mechanism.

During the first 350 ps of this cv-SMD simulation, the ligand rotated counterclockwise by 90° with the sulfur atom pointing out of the binding pocket (Figure 3 and Figure S5). At that time, the benzene ring **2** induced a counterclockwise rotation of U23 of the χ-dihedral by 50° and the benzene ring **2** stacked on U23, sulfur atom formed a van der Waals interaction with U25, the aliphatic chain induced a rotation of the χ-dihedral of C24 from -75° to -165°, A22

shifted by 40°, partially flipping out and providing space to C24 to rotate and flip inward, following the movement of the ligand out of the binding pocket.

At a distance of 5.6 Å (t = 450 ps), the sulfur atom continued to interact with U25 that resulted in an intramolecular conformational change in the ligand where three fused aromatic rings formed ∼90° angle with the aliphatic chain (Figure 3 and Figure S5). In the meantime, C24 flipped inward, occupying the free space left behind by the ligand, and formed a hydrogen bond with the oxygen atom of U40 while A22 returned to its initial position in the RNA stack. The flipping of C24 back into the RNA helix represents a rare base-flipping event in nucleic acids that occurs on a millisecond timescale and is difficult to observe both experimentally and during conventional MD simulations.[38,39]

Between 450 ps and 800 ps, U23 flipped underneath the ligand that was moving out of the pocket, thus making a pathway free of any obstacles (Figure 3 and Figure S5). At a distance of 9.55 Å (800 ps), the ligand rotated again causing a minor counterclockwise rotation of U25 around the χ-dihedral by 60°. As the ligand was dissociating, U23 moved out of the binding pocket and flipped out when the ligand was at a distance of 10 Å away from U23. The ligand was free of any interactions with the RNA at d = 17.5 Å. Other simulations with lower work values indicated a similar mechanism of ligand dissociation (Figure S6).

In contrast, in the simulation trajectory resulting in the highest dissociation work, the C24 nucleotide did not flip inside, despite interacting with the ligand as in the lowest work simulation (Figure 3 and Figure S7). This could be potentially explained by the fact that A22 did not shift to provide additional space for C24. At 360 ps, the base part of U25 rotated around the χ-dihedral by 100° while still interacting with the sulfur atom of the ligand. In addition to that, U23 did not interact with benzene ring **2** as long as it did in the lowest work simulation and did not move closer to A22 below the ligand. Instead, when U25 was rotating, U23 got shifted away from the ligand and stacked on U25 for ∼120 ps. That transition moved U23 in the outward configuration with respect to the binding pocket and above the ligand, while in the lowest work simulation U23 was below the ligand toward the

binding pocket.

At 500 ps, U25 started interacting with the sulfur atom of the ligand which caused a rotation of the nucleobase in U23 around the χ-dihedral from -150° to 60° (Figure 4A). U23 proceeded to interact with the ligand by stacking on the benzene ring **2** between 500 ps and 950 ps which resulted in the rotation of U23 base to its original χ-dihedral value of -150° (Figure 4A). U23 then interacted with the aliphatic chain and remained in the flipped out state for the remainder of the simulation. These sequence of events potentially contribute to additional work required to overcome more stacking interactions between the acetylpromazine benzene ring **2** and U23/U25. Also, after the ligand moved out of the binding pocket, it continued to interact with A35 that was flipped out in the stem-loop of RNA (Figure S8).

Mechanistic Details of Ligand Dissociation: To characterize the conformational rearrangements of the binding pocket nucleotides in the least work simulation, including the flipping-in of C24, and probe the reasons for not observing this flipping event in the highest work simulation, we describe a number of mechanistic details that collectively describe these events. These details can further improve our understanding of a base flipping process in TAR-RNA and in bulge motifs of RNA in general.

We observed a sequence of conformational transitions in U23 and U25 (Figure S9) that influenced the base flipping as well as potentially contributed to the amount of work needed to dissociate the ligand. As highlighted in earlier discussion, U23 rotated around the χ-dihedral and buried deeper in the binding pocket in the first 350 ps in the least work simulation. The movement of A22 outward was a consequence of this transition since U23 was displaced by the ligand which in turn displaced A22. Between 350 ps and 1000 ps, U23 rotated relative to A22 (Figure S10A) by 100° and moved away from U25 by 2 Å (Figure 4B) while partially filling the space that was available after A22 moved outward. At ∼830 ps, U25 rotated around the χ-dihedral by 40° counterclockwise and interacted with U23 until it (U23) flipped out at the end of the simulation. Interestingly, in the highest work simulation the same base

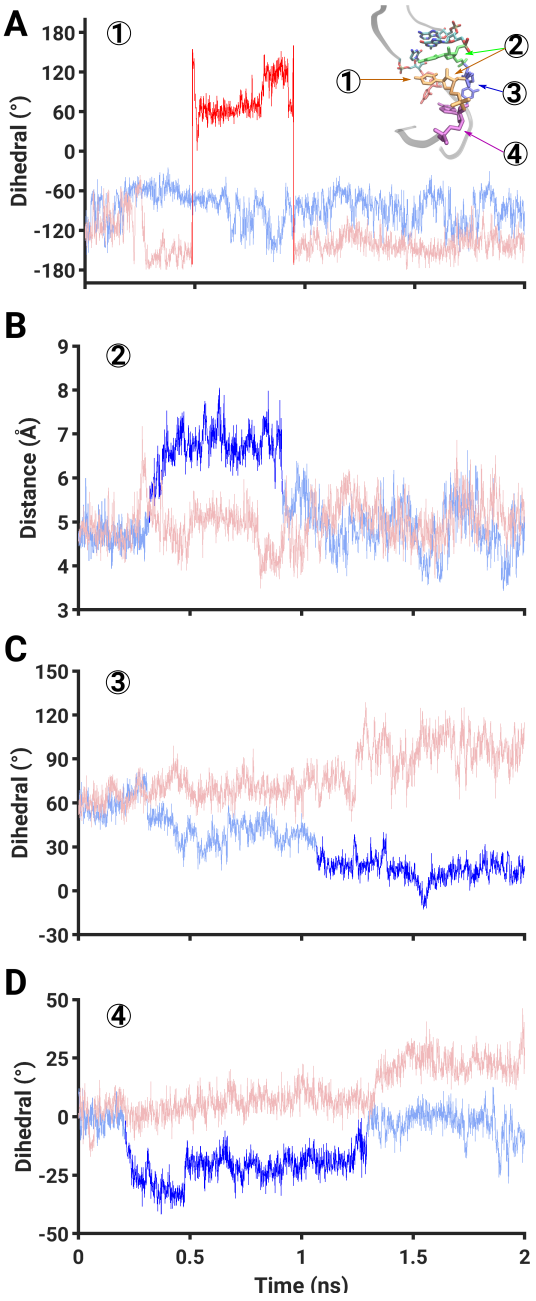

Figure 4: Conformational metrics : Shown are the traces of several conformational metrics from the lowest work (blue) and the highest work (red) simulations. Darker colors signify transition regions of interest. The numbers in each panel correspond to metrics computed for specific nucleotides (see *inset* in panel A). The conformational metrics shown are: (A) χ-dihedral of U23 nucleotide; (B) distance between the COM of U23 and U25; (C) dihedral angle that describes the flipping of C24; and (D) dihedral angle that describes the rotation of A22. See also Figure S10.

rotated around the χ-dihedral in the opposite direction by 120°. Also, in that simulation, U23 rotated clockwise (opposite to the direction of rotation in the lowest work simulation where U23 moved inside the binding pocket) by 90° around the χ-dihedral at 350 ps which caused it to move out of the binding pocket. The difference in the directions of rotation of the χ-dihedral of U23 is a crucial detail that led to different conformational events in the binding pocket and likely influenced the final work values.

As shown in Figure 4C, the flipping in of C24 toward the binding pocket started after the rotation around its χ-dihedral which was observed in both the lowest and the highest work simulations. However, only in the lowest work simulation, this rotation was followed by the transition to an inward conformation. At 350 ps, A22 shifted in the outward direction by 30° counterclockwise (Figures 4D and S11) providing space for C24 to move in. In the highest work simulation, on the contrary, A22 did not shift outward, remaining at its initial position and forming a base pair with U40 after the ligand dissociated.

In the lowest work simulation, the movement of A22 outward was followed by the movement of C24 inward as described by the dihedral-angle in Figure 4C at ∼400 ps. We observed fluctuations in C24 as it was moving in because the ligand had to first leave the binding pocket and provide space for that nucleotide. It also started to form a hydrogen bond with U40 (Figure S10B and S11) and after the ligand completely dissociated, the hydrogen bond was stabilized (after 1 ns). Thus, C24 replaced the ligand which acted as a "pseudo base pair" in the initial conformation between A22 and U40. This highlights that ligands recognized by RNA likely substitute for and conformationally mimic interactions between RNA nucleobases.

Binding/unbinding of ligands in RNA systems is an important biophysical process that is poorly understood. We used non-equilibrium cv-SMD and conventional MD simulations to study the dissociation pathway of acetylpromazine from TAR-RNA binding pocket to obtain key insights into the ligand binding/unbinding process. As expected, we did not observe ligand dissociation in a conventional MD simulation. On the contrary, cv-SMD

simulations facilitated ligand dissociation and provided a large ensemble of trajectories to study this mechanism. In particular, we investigated in detail the lowest and the highest work simulations to identify mechanistic underpinnings of ligand dissociation. In the simulation with the lowest work value, we observed a rare base flipping event in the C24 nucleotide of TAR-RNA. This transition was a result of a sequence of complex events relating 5 nucleotides that were not observed in the highest work simulation.

Interestingly, the differences in the sequence of events between the lowest and the highest work simulations were initiated by the rotation of the χ-dihedral of U23 in opposite directions which we have identified for the first time. The counterclockwise rotation of the χ-dihedral of U23 not only decreased the amount of work but assisted in flipping-in of C24. We suggest that building a substantial ensemble of non-equilibrium trajectories is a potentially useful approach to gain insights into rare conformational transitions. These simulations, together with the Jarzynski's equality, were also able to predict the bounds on K_d within which was the experimentally measured value. Furthermore, we reported mechanistic details underlying several conformational transitions, including a dihedral-angle of C24, a hydrogen bond between C24 and U40, the χ-dihedral of U23, and an interplane angle between U23 and A22. Since the transitions in these variables exhibit two-state features, it is potentially useful to invoke rare event sampling methods to further study this mechanism in future. Specifically, transition path sampling[40,41] along with the likelihood maximization[42,43] is an exhaustive and accurate method to study these types of events. Its principles have been applied to study protein[44] and RNA systems.[45] Moreover, conformational transitions observed here can be potentially exploited for designing a new generation of inhibitory molecules targeting TAR-RNA.

Experimental Methods

We conducted MD and SMD simulations of HIV-1 TAR-RNA in complex with the ligand acetylpromazine. We used the AMBER force-field with the AMBER, NAMD, and VMD

software packages.[46–53]Additional details are provided in the Supporting Information.

Acknowledgement

We acknowledge financial support from the National Science Foundation (CBET-1554558) and computational support through the following resources: Premise, a central shared HPC cluster at UNH supported by the Research Computing Center; BioMade, a heterogeneous CPU/GPU cluster supported by the NSF EPSCoR award (OIA-1757371); and the NSF-supported (ACI-1548562) Extreme Science and Engineering Discovery Environment (XSEDE) Comet resource at San Diego Supercomputer Center (SDSC) under grant TG-MCB160183 (HV).

Supporting Information

Supplemental methods and 11 figures are described in the Supporting Information.

References

(1) Nissen, P.; Hansen, J.; Ban, N.; Moore, P. B.; Steitz, T. A. The structural basis of ribosome activity in peptide bond synthesis. *Science* **2000**, *289*, 920–930.

(2) Cech, T.; Steitz, J. The noncoding RNA revolution-trashing old rules to forge new ones. *Cell* **2014**, *157*, 77–94.

(3) Sharp, P. A. The centrality of RNA. *Cell* **2009**, *136*, 577–580.

(4) Fedor, M. J.; Williamson, J. R. The catalytic diversity of RNAs. *Nat. Rev. Mol. Cell Biol.* **2005**, *29*, 399–412.

(5) Angelbello, A. J.; Chen, J. L.; Disney, M. D. Small molecule targeting of RNA structures in neurological disorders. *Ann. N. Y. Acad. Sci.* **2019**, *XXX*, 1–15.

(6) Schmitt, A. M.; Chang, H. Y. Long noncoding RNAs in cancer pathways. *Cancer Cell* **2016**, *6*, 452–463.

(7) Laina, A.; Gatsiou, A.; Georgiopoulos, G.; Stamatelopoulos, K.; Stellos, K. RNA therapeutics in cardiovascular precision medicine. *Front. Physiol.* **2018**, *123*, 205—-220.

(8) Freed, E. O. HIV-1 assembly, release and maturation. *Nat. Rev. Microbiol.* **2015**, *13*, 484–496.

(9) Kieft, J. S.; Zhou, K.; Jubin, R.; Doudna, J. A. Mechanism of ribosome recruitment by hepatitis C IRES RNA. *RNA* **2001**, *7*, 194–206.

(10) Plant, E. P.; Dinman, J. D. The role of programmed-1 ribosomal frameshifting in coronavirus propagation. *Front. Biosci.* **2008**, *13*, 4873–4881.

(11) Warner, K.; Hajdin, C.; Weeks, K. Principles for targeting RNA with drug-like small molecules. *Nat. Rev. Drug Discovery* **2018**, *17*, 547–558.

(12) Hermann, T. *Viral RNA targets and their small molecule ligands*, RNA Therapeutics. Topics in Medicinal Chemistry ed.; Springer, Cham, 2017; Vol. 27.

(13) Patwardhan, N. N.; Ganser, L. R.; Kapral, G. J.; Eubanks, C. S.; Lee, J.; Sathyamoorthy, B.; Al-Hashimi, H. M.; Hargrove, A. E. Amiloride as a new RNA-binding scaffold with activity against HIV-1 TAR. *Med. Chem. Commun.* **2017**, *8*, 1022–1036.

(14) Patwardhan, N. N.; Cai, Z.; Juru, A. U.; Hargrove, A. E. Driving factors in amiloride recognition of HIV RNA targets. *Org. Biomol. Chem.* **2019**, *17*, 9313–9320.

(15) Disney, M. D.; Yildirim, I.; Childs-Disney, J. L. Methods to enable the design of bioactive small molecules targeting RNA. *Org. Biomol. Chem.* **2014**, *12*, 1029–1039.

(16) Juru, A. U.; Patwardhan, N. N.; Hargrove, A. E. Understanding the contributions of conformational changes, thermodynamics, and kinetics of RNA-small molecule interactions. *ACS Chem. Biol.* **2019**, *14*, 824–838.

(17) Zhang, Q.; Sun, X.; Watt, E. D.; Al-Hashimi, H. M. Resolving the motional modes that code for RNA adaptation. *Science* **2006**, *311*, 653–656.

(18) Al-Hashimi, H. M. NMR studies of nucleic acid dynamics. *J. Magn. Reson.* **2013**, *237*, 191–204.

(19) Do, P.-C.; Lee, E. H.; Le, L. Steered molecular dynamics simulation in rational drug design. *J. Chem. Inf. Model.* **2018**, *58*, 1473–1482.

(20) Salmon, L.; Yang, S.; Al-Hashimi, H. M. Advances in the determination of nucleic acid conformational ensembles. *Annu. Rev. Phys. Chem.* **2014**, *65*, 293–316.

(21) Salmon, L.; Giambaşu, G. M.; Nikolova, E. N.; Petzold, K.; Case, A. B. D. A.; Al-Hashimi, H. M. Modulating RNA alignment using directional dynamic kinks: application in determining an atomic-resolution ensemble for a hairpin using NMR residual dipolar couplings. *J. Am. Chem. Soc.* **2015**, *137*, 12954–12965.

(22) Ganser, L. R.; Kelly, M. L.; Al-Hashimi, D. H. H. M. The roles of structural dynamics in the cellular functions of RNAs. *Nat. Rev. Mol. Cell. Biol.* **2019**, *20*, 474–489.

(23) Ettig, R.; Kepper, N.; Stehr, R.; Wedemann, G.; Rippe, K. Dissecting DNA-histone interactions in the nucleosome by molecular dynamics simulations of DNA unwrapping. *Biophys. J.* **2011**, *101*, 1999–2008.

(24) Gupta, A.; Bansal, M. The role of sequence in altering the unfolding pathway of an RNA pseudoknot: a steered molecular dynamics study. *Phys. Chem. Chem. Phys.* **2016**, *18*, 28767–28780.

(25) Vashisth, H.; Abrams, C. F. Ligand escape pathways and (un)binding free energy calculations for the hexameric insulin-phenol complex. *Biophys. J.* **2008**, *95*, 4193–4204.

(26) Capelli, A. M.; Costantino, G. Unbinding pathways of VEGFR2 inhibitors revealed by steered molecular dynamics. *J. Chem. Inf. Model.* **2014**, *54*, 3124–3136.

(27) Palma, F. D.; Colizzi, F.; Bussi, G. Ligand-induced stabilization of the aptamer terminal helix in the add adenine riboswitch. *RNA* **2013**, *19*, 1517–1524.

(28) Do, T. N.; C, P.; Varani, G.; Bussi, G. RNA/peptide binding driven by electrostatics-insight from bidirectional pulling simulations. *J. Chem. Theory Comput.* **2013**, *9*, 1720–1730.

(29) Zonta, F.; Buratto, D.; Cassini, C.; Bortolozzi, M.; Mammano, F. Molecular dynamics simulations highlight structural and functional alterations in deafness-related M34T mutation of connexin 26. *Front. Physiol.* **2014**, *5*, 85.

(30) Nishihara, Y.; Kitao, A. Gate-controlled proton diffusion and protonation-induced ratchet motion in the stator of the bacterial flagellar motor. *Proc. Natl. Acad. Sci. U.S.A.* **2015**, *112*, 7737–7742.

(31) Dethoff, E. A.; Petzold, K.; Chugh, J.; Casiano-Negroni, A.; Al-Hashimi, H. M. Visualizing transient low-populated structures of RNA. *Nature* **2012**, *491*, 724–728.

(32) Bannwarth, S.; Gatignol, A. HIV-1 TAR RNA: the target of molecular interactions between the virus and its host. *Curr. HIV Res.* **2005**, *3*, 61–71.

(33) Du, Z.; Lind, K. E.; James, T. L. Structure of TAR RNA complexed with a Tat-TAR interaction nanomolar inhibitor that was identified by computational screening. *Chem. Biol.* **2002**, *9*, 707–712.

(34) Jarzynski, C. Nonequilibrium equality for free energy differences. *Phys. Rev. Lett.* **1997**, *78*, 2690–2693.

(35) Jensen, M.; Park, S.; Tajkhorshid, E.; Schulten, K. Energetics of glycerol conduction through aquaglyceroporin GlpF. *PNAS* **2002**, *99*, 6731–6736.

(36) Park, S.; Khalili-Araghi, F.; Tajkhorshid, E.; Schulten, K. Free energy calculation

from steered molecular dynamics simulations using Jarzynski's equality. *J. Chem. Phys.* **2003**, *119*, 3559–3566.

(37) Park, S.; Schulten, K. Calculating potentials of mean force from steered molecular dynamics simulations. *J. Chem. Phys.* **2004**, *120*, 5946–5961.

(38) Snoussi, K.; Leroy, J. L. Imino proton exchange and base-pair kinetics in RNA duplexes. *Biochemistry* **2001**, *40*, 8898–8904.

(39) Yin, Y.; Yang, L.; Zheng, G.; Gu, C.; Yi, C.; He, C.; Gao, Y. Q.; Zhao, X. S. Dynamics of spontaneous flipping of a mismatched base in DNA duplex. *Proc. Natl. Acad. Sci. U.S.A.* **2014**, *111*, 8043–8048.

(40) Bolhuis, P. G.; Chandler, D.; Dellago, C.; Geissler, P. L. Transition path sampling: throwing ropes over rough mountain passes, in the dark. *Annu. Rev. Phys. Chem.* **2002**, *53*, 291–318.

(41) Peters, B. Reaction coordinates and mechanistic hypothesis tests. *Annu. Rev. Phys. Chem.* **2016**, *67*, 669–690.

(42) Peters, B.; Trout, B. L. Obtaining reaction coordinates by likelihood maximization. *J. Chem. Phys.* **2006**, *125*, 054108.

(43) Peters, B. Extensions to the likelihood maximization approach for finding reaction coordinates. *J. Chem. Phys.* **2007**, *127*, 034109.

(44) Freitas, F. C.; Lima, A. N.; de Godoi Contessoto, V.; Whitford, P. C.; de Oliveira, R. J. Drift-diffusion (DrDiff) framework determines kinetics and thermodynamics of two-state folding trajectory and tunes diffusion models. *J. Chem. Phys.* **2019**, *151*, 114106.

(45) Levi, M.; Whitford, P. C. Dissecting the energetics of subunit rotation in the ribosome. *J. Phys. Chem. B* **2019**, *123*, 2812–2823.

(46) Perez, A.; Marchan, I.; Svozil, D.; Sponer, J.; Cheatham, T. E.; Laughton, C. A.; Orozco, M. Refinement of the AMBER force field for nucleic acids: improving the description of alpha/gamma conformers. *Biophys. J.* **2007**, *92*, 3817–3829.

(47) Zgarbova, M.; Otyepka, M.; Sponer, J.; Mladek, A.; Banas, P.; Cheatham, T. E.; Jurecka, P. Refinement of the Cornell et al. nucleic acids force field based on reference quantum chemical calculations of glycosidic torsion profiles. *J. Chem. Theory Comput.* **2011**, *7*, 2886–2902.

(48) Salomon-Ferrer, R.; Case, D. A.; Walker, R. C. An overview of the Amber biomolecular simulation package. *WIREs Comput. Mol. Sci.* **2013**, *3*, 198–210.

(49) Phillips, J. C.; Braun, R.; Wang, W.; Gumbart, J.; Tajkhorshid, E.; Villa, E.; Chipot, C.; Skeel, R. D.; Kale, L.; Schulten, K. Scalable molecular dynamics with NAMD. *J. Comput. Chem.* **2005**, *26*, 1781–1802.

(50) Wang, J.; Wang, W.; Kollman, P. A.; Case, D. A. Automatic atom type and bond type perception in molecular mechanical calculations. *J. Mol. Graph. Model.* **2006**, *25*, 247–260.

(51) Wang, J.; Wolf, R. M.; Caldwell, J. W.; Kollman, P. A.; Case, D. A. Development and testing of a general amber force field. *J. Comput. Chem.* **2004**, *25*, 1157–1174.

(52) Wang, J.; Wolf, R. M.; Caldwell, J. W.; Kollman, P. A.; Case, D. A. Fast, efficient generation of high-quality atomic charges. AM1-BCC model: II. Parameterization and validation. *J. Comput. Chem.* **2002**, *23*, 1623–1641.

(53) Humphrey, W.; Dalke, A.; Schulten, K. VMD: visual molecular dynamics. *J. Molec. Graphics* **1996**, *14*, 33–38.